INTERNATIONAL JOURNAL FOR NUMERICAL METHODS IN ENGINEERING
Int. J. Numer. Meth. Engng 2007; **69**:308–325
Published online 5 June 2006 in Wiley InterScience (www.interscience.wiley.com). DOI: 10.1002/nme.1762

High-order DGTD methods for dispersive Maxwell's equations and modelling of silver nanowire coupling

Xia Ji[1,‡], Wei Cai[2,*,†] and Pingwen Zhang[1,§]

[1]*LMAM and School of Mathematical Sciences, Peking University, Beijing 100871, China*
[2]*Department of Mathematics, Center for Optoelectronics and Optical Communications, University of North Carolina at Charlotte, Charlotte, NC 28223, U.S.A.*

SUMMARY

A high-order discontinuous Galerkin time-domain (DGTD) method for Maxwell's equations for dispersive media of Drude type is derived and then used to study the coupling of 2D silver nanowires, which have potential applications in optical circuits without the restriction of diffraction limits of traditional dielectric waveguides. We have demonstrated the high accuracy of the DGTD for the electromagnetic wave scattering in dispersive media and its flexibility in modelling the plasmon resonant phenomena of coupled silver nanowires. Specifically, we study the cross sections of coupled nanowires, the dependence of the resonance on the number of nanowires with more resolved resonance information than the traditional FDTD Yee scheme, time-domain behaviour of waves impinging on coupled silver nanowires of a funnel configuration, and the energy loss of resonant modes in a linear chain of circular and ellipse nanowires. Copyright © 2006 John Wiley & Sons, Ltd.

Received 15 September 2005; Revised 23 March 2006; Accepted 24 March 2006

KEY WORDS: discontinuous Galerkin time-domain (DGTD); Maxwell's equations; plasmon; resonance; nanowires

*Correspondence to: Wei Cai, Department of Mathematics, University of North Carolina at Charlotte, Charlotte, NC 28223, U.S.A.
†E-mail: wcai@uncc.edu
‡E-mail: jixia@math.pku.edu.cn
§E-mail: pzhang@math.pku.edu.cn

Contract/grant sponsor: US National Science Foundation and Department of Energy; contract/grant numbers: DMS-0408309, CCF-0513179, DEFG0205ER25678
Contract/grant sponsor: National Science Foundation of China and Grant for Distinguished Young Scholars; contract/grant numbers: 90207009, 10225103
Contract/grant sponsor: NERSC Computing Award

1. INTRODUCTION

There has been increasing research activities in the area of nano-optics for applications in optical circuits and nanoscale devices. The motivation is to overcome the diffraction limit of light propagation in traditional dielectric optical fibres and photonic waveguides such as CROWs [1]. Metal waveguides and metallic nanostructures have attracted much attention in providing such a solution to overcome the diffraction limit using so-called 'low-dimensional optical waves' [2]. The low-dimensional optical waves are produced by surface polariton plasmon (SPP) waves along metal/dielectric interfaces or metal films between dielectrics. The SSP wave is a type of evanescent waves confined to interfaces, which result from the interaction of electromagnetic waves and electrons in resonance in metals. Such an interaction also indicates a strongly frequency dependence for the metal permittivity $\varepsilon(\omega)$. In general, the real part of the ε will change sign as the frequency ω crosses the plasmon frequency ω_{p}. Such a frequency dependence brings challenges to accurate numerical studies of the SPP waveguides. In Reference [3], it was shown using numerical approximation based on Mie series that electromagnetic energy could be transported successfully through linear chain of silver nanoparticles. Such a transport was made possible from the near field interaction between nanowires through the coupled dipole or plasmon modes [4]. Recently, Gray *et al.* has used a finite difference time-domain (FDTD) Yee scheme to study the transient propagation of light through coupled silver nanowires [5]. Other numerical studies of coupled nanowires have been done with the solution of frequency domain Maxwell equations [6–10].

Due to the small scales of the nanostructures and evanescent nature of the SPP waves, accurate modelling of optical circuits demands high-order accuracy of the numerical methods, especially the phase accuracy for light propagation. In this paper, following Reference [11], we will derive a high-order discontinuous Galerkin time-domain (DGTD) method for electromagnetic waves in dispersive media of Drude type, which will then be applied to study silver nanowires. Previous studies on DGTD for electromagnetic scattering can be found in References [12, 13]. To our knowledge, this is the first time the DGTD method for dispersive Maxwell's equations is used to study a dispersive metal system. Our numerical study of coupled silver nanowires with this high-order method has produced clearer picture of the resonant frequency information than those by the second-order FDTD Yee scheme employed in Reference [5]. We believe this is a direct result of the high-order accuracy in our DGTD method, which treats the geometric information of the nanowire explicitly with a finite element-type mesh, and the frequency dependency of the dielectric constant with the ADE method [11, 14], and the high-order polynomial basis functions to represent the exponentially variant field near the interfaces. The commonly used Yee scheme, while simple to be implemented on a Cartesian finite difference grid, lacks the necessary accuracy near material interfaces between dielectric and metals.

Using the high-order DGTD method, we will carry a systematic study of the plasmon resonant coupling of silver nanowires. In Section 2, we will derive the DGTD method for Maxwell's system in a Drude-type dispersive medium. Section 3 will contain the study of the cross sections of coupled silver nanowires and the dependence of the resonance on the number of nanowires in a linear chain [15] while Section 4 will present the energy loss of resonant modes in a linear chain of different type of silver nanowires [3, 16]. Finally, Section 5 will give the conclusion.

DOI: 10.1002/nme

2. UNIFIED FORMULATION FOR DISPERSIVE MAXWELL'S EQUATIONS AND DGTD

2.1. Unified formulation for dispersive Maxwell's equations in physical regions and UPML regions

The systems considered are lossy and dispersive, we consider a single-pole Drude medium [17], whose relative electric permittivity can be written as

$$\varepsilon_r(\omega) = \varepsilon_{r,\infty} - \frac{\omega_p^2}{\omega^2 + i\gamma\omega}$$

where ω_p is the plasma frequency, γ is the damping constant, $\varepsilon_{r,\infty}$ is the relative electric permittivity at infinite frequency. The frequency dependence of permittivity implies a time convolution between the displacement field $\mathbf{D}$ and the electric field $\mathbf{E}$, the auxiliary differential equation (ADE) method [11, 14] is used to address this problem with the help of polarization currents.

We consider a non-dimensionalized form of Maxwell's equations for TE cases (in two-dimensional problems surface plasmons can only be excited in TE cases [18]) in physical regions and UPML regions [11] by introducing non-dimensionalized variables:

$$\begin{aligned} &\frac{x}{L} \to x, \quad \frac{y}{L} \to y, \quad \frac{ct}{L} \to t \\ &Z_0\mathbf{H} \to \mathbf{H}, \quad \mathbf{E} \to \mathbf{E} \end{aligned} \tag{1}$$

where L is the reference length associated with a given problem, and c is the speed of light in the free space, $Z_0 = (\mu_0/\varepsilon_0)^{1/2}$ is the free-space impedance.

The augmented Maxwell's equations with auxiliary polarization currents for the new augmented variables $\mathbf{U} = (\mu_r H_z, \varepsilon_{r,\infty} E_x, \varepsilon_{r,\infty} E_y, Q_z, P_{x,2}, P_{x,3}, P_{x,4}, P_{y,2}, P_{y,3}, P_{y,4})^{\mathrm{T}}$ are

$$\frac{\partial \mathbf{U}}{\partial t} + \nabla \cdot (\bar{\mathbb{A}}\mathbf{U}) = \mathbf{S} \tag{2}$$

where $\bar{\mathbb{A}}$ and $\mathbf{S}$ are given below. We can divide the above conservation system into two parts

$$\frac{\partial \mathbf{U}^{(1)}}{\partial t} + \nabla \cdot (\mathbb{A}\mathbf{U}^{(1)}) = \mathbf{S}^{(1)} \tag{3}$$

$$\frac{\partial \mathbf{U}^{(2)}}{\partial t} = \mathbf{S}^{(2)} \tag{4}$$

where $\mathbf{U}^{(1)} = (\mu_r H_z, \varepsilon_{r,\infty} E_x, \varepsilon_{r,\infty} E_y)^{\mathrm{T}}$, $\mathbf{U}^{(2)} = (Q_z, P_{x,2}, P_{x,3}, P_{x,4}, P_{y,2}, P_{y,3}, P_{y,4})^{\mathrm{T}}$, $\mathbf{U} = (\mathbf{U}^{(1)}, \mathbf{U}^{(2)})^{\mathrm{T}}$, $\mathbf{S} = (\mathbf{S}^{(1)}, \mathbf{S}^{(2)})^{\mathrm{T}}$ and $\mathbb{A} = (A_x, A_y)$, where

$$A_x = \begin{pmatrix} 0 & 0 & 1/\varepsilon_{r,\infty} \\ 0 & 0 & 0 \\ 1/\mu_r & 0 & 0 \end{pmatrix}, \quad A_y = \begin{pmatrix} 0 & -1/\varepsilon_{r,\infty} & 0 \\ -1/\mu_r & 0 & 0 \\ 0 & 0 & 0 \end{pmatrix} \tag{5}$$

DOI: 10.1002/nme

Meanwhile, $\bar{\mathbb{A}}$ is given as

$$\bar{\mathbb{A}} = (\bar{A}_x, \bar{A}_y)$$

where

$$\bar{A}_x = \begin{pmatrix} A_x & 0_{3\times 7} \\ 0_{7\times 3} & 0_{7\times 7} \end{pmatrix}, \quad \bar{A}_y = \begin{pmatrix} A_y & 0_{3\times 7} \\ 0_{7\times 3} & 0_{7\times 7} \end{pmatrix}$$

Here $0_{n\times m}$ denotes zero matrix with n rows and m columns. The source terms $\mathbf{S}^{(1)}$ and $\mathbf{S}^{(2)}$ represent body forces, e.g. polarization currents,

$$\mathbf{S}^{(1)} = -\begin{pmatrix} \mu_r d_{0,z} H_z + \mu_r d_{1,z} Q_z, \\ \varepsilon_{r,\infty} c_{1,x} E_x + \omega_p^2 P_{x,4} + \omega_p^2 c_{1,x} P_{x,3} + c_{2,x} P_{x,2}, \\ \varepsilon_{r,\infty} c_{1,y} E_y + \omega_p^2 P_{y,4} + \omega_p^2 c_{1,y} P_{y,3} + c_{2,y} P_{y,2} \end{pmatrix} \tag{6}$$

$$\mathbf{S}^{(2)} = \begin{pmatrix} H_z, \\ \omega_p^2 P_{x,3} + \varepsilon_{r,\infty} E_x - \sigma_x P_{x,2} \\ P_{x,4} \\ E_x - \gamma P_{x,4} \\ \omega_p^2 P_{y,3} + \varepsilon_{r,\infty} E_y - \sigma_y P_{y,2} \\ P_{y,4} \\ E_y - \gamma P_{y,4} \end{pmatrix} \tag{7}$$

where

$$\begin{aligned} c_{1,x} &= \sigma_y - \sigma_x, \quad c_{2,x} = -\sigma_x(\sigma_y - \sigma_x) \\ c_{1,y} &= \sigma_x - \sigma_y, \quad c_{2,y} = -\sigma_y(\sigma_x - \sigma_y) \\ d_{0,z} &= \sigma_x + \sigma_y, \quad d_{1,z} = \sigma_x \sigma_y \end{aligned} \tag{8}$$

The equations above are reduced to the usual Maxwell's equations in the physical media when the UPML parameters $\sigma_x = 0$, $\sigma_y = 0$. The P's and Q's above are the auxiliary polarization variables used to handle the temporal convolution of the electromagnetic fields of the UPML regions and the dispersive constitutive relations. We usually allow the UPML losses $\sigma_x(x)$ to have a polynomial profile [14]

$$\sigma_x(x) = (l/\Delta)^m \sigma_{x,\max} \tag{9}$$

where l is the distance from the interface between the UPML and the physical solution domain, and Δ is the thickness of the UPML. The definition of $\sigma_y(y)$ is similar. The reflection factor

DOI: 10.1002/nme

for the UPML is

$$R(\theta) = \exp\{-2\eta\sigma_{x,\max}\Delta\cos\theta/[\varepsilon_{r,\infty}(m+1)]\} \tag{10}$$

where θ is the incident angle, and η is the UPML's characteristic wave impedance.

2.2. Discontinuous Galerkin time-domain (DGTD) method

To solve Equation (2) in general geometries, we divide the solution domain Ω into non-overlapping quadrilateral and/or triangular elements, let $\mathscr{T}_h$ be a discretization of the solution domain. On each element $K \in \mathscr{T}_h$, $\varepsilon_{r,\infty}$ and μ_r are assumed to be constant. Each physical element K is then mapped by an isoparametric transformation [19] onto a reference element I, which is either a reference square $[-1, 1]^2$ or a reference triangle $\{(x, y)|, 0\leqslant x, y\leqslant 1, 0\leqslant x + y\leqslant 1\}$.

We will use a finite-dimensional space of smooth functions (polynomials for DGTD methods, denoted by $\mathscr{P}(K)$) to approximate the variable $\mathbf{U}$. Defining

$$V_h := \{v \in L^1(\Omega) \mid v|_K \in \mathscr{P}(K)\ \forall K \in \mathscr{T}_h\} \tag{11}$$

and

$$V_h^{10} := \underbrace{V_h \times V_h \times \cdots \times V_h}_{10} \tag{12}$$

We can obtain the DGTD space discretization of the hyperbolic system Equations (3) and (4) as follows. Find $\mathbf{U} \in V_h^{10}$ such that for all $v_h \in V_h$

$$\int_K \left(\frac{\partial \mathbf{U}^{(1)}}{\partial t} v_h - \mathbf{S}^{(1)} v_h - \mathbb{A}\mathbf{U}^{(1)} \cdot \nabla v_h\right) \mathrm{d}\mathbf{x} + \int_{\partial K} \mathbf{h}_K(\mathbf{U}^{(1),-}, \mathbf{U}^{(1),+}) v_h \,\mathrm{d}s = 0 \tag{13}$$

$$\int_K \left(\frac{\partial \mathbf{U}^{(2)}}{\partial t} v_h - \mathbf{S}^{(2)} v_h\right) \mathrm{d}\mathbf{x} = 0 \tag{14}$$

where $\hat{\mathbf{n}}_K = (n_x, n_y)$ is the outward unit normal to ∂K, $\mathbf{U}^{(1),-}$ and $\mathbf{U}^{(1),+}$ are defined as

$$\mathbf{U}^{(1),\pm}(\mathbf{x}) = \lim_{\delta \to 0^+} \mathbf{U}^{(1)}(\mathbf{x} \pm \delta \hat{\mathbf{n}}_k)$$

as $\mathbf{U}$ is in general discontinuous across ∂K. The numerical flux $\mathbf{h}_K(\mathbf{U}^{(1),-}, \mathbf{U}^{(1),+})$ is an approximation to $\hat{\mathbf{n}}_K \cdot \mathbb{A}\mathbf{U}^{(1)}|_{\partial K}$ on the faces of the element K, and should satisfy the following consistent condition:

$$\mathbf{h}_K(\mathbf{U}^{(1)}, \mathbf{U}^{(1)}) = \hat{\mathbf{n}}_K \cdot \mathbb{A}\mathbf{U}^{(1)}|_{\partial K} \tag{15}$$

DOI: 10.1002/nme

We can obtain $\mathbf{h}_K(\mathbf{U}^{(1),-}, \mathbf{U}^{(1),+})$ by solving a local Riemann problem [11, 20], the numerical flux $\mathbf{h}_K(\mathbf{U}^{(1),-}, \mathbf{U}^{(1),+})$ for the 2D TE Maxwell's equations is

$$\mathbf{h}_K(\mathbf{U}^{(1),-}, \mathbf{U}^{(1),+}) = \left\{ \begin{array}{c} \dfrac{[Y(n_x E_y - n_y E_x) + H_z]^- + [Y(n_x E_y - n_y E_x) - H_z]^+}{Y^- + Y^+} \\ -n_y \dfrac{[ZH_z + (n_x E_y - n_y E_x)]^- + [ZH_z - (n_x E_y - n_y E_x)]^+}{Z^- + Z^+} \\ n_x \dfrac{[ZH_z + (n_x E_y - n_y E_x)]^- + [ZH_z - (n_x E_y - n_y E_x)]^+}{Z^- + Z^+} \end{array} \right\}$$

$$= \left\{ \begin{array}{c} h_K^{H_z} \\ h_K^{E_x} \\ h_K^{E_y} \end{array} \right\}$$

where $Z^{\pm}$ and $Y^{\pm}$ are the local impedance and admittance, respectively, defined as

$$Z^{\pm} = 1/Y^{\pm} = (\mu_r^{\pm}/\varepsilon_r^{\pm})^{1/2}$$

and $\mathbf{U}^{(1)} = (\mu_r H_z, \varepsilon_{r,\infty} E_x, \varepsilon_{r,\infty} E_y)^{\mathrm{T}}$.

2.3. Space discretization

Let $\{\phi_j(x)\}_{j=1}^N$ be the basis function of the polynomial space $\mathscr{P}(K)$ defined in Reference [11], we can expand the magnetic field H_z, and the electric fields E_x and E_y in terms of the basis functions $\phi_j(\mathbf{x})$,

$$H_{z,N}(\mathbf{x}, t) = \sum_{j=1}^{N} H_{z,j} \phi_j(\mathbf{x}) \tag{16}$$

$$E_{s,N}(\mathbf{x}, t) = \sum_{j=1}^{N} E_{s,j} \phi_j(\mathbf{x}), \quad s = x, y \tag{17}$$

where $H_{z,j}$ and $E_{x,j}$, $E_{y,j}$ are functions of time. We also project $\mathbf{U}^{(2)}$ to the function space expanded by the basis functions,

$$Q_{z,N}(\mathbf{x}, t) = \sum_{j=1}^{N} Q_{z,j} \phi_j(\mathbf{x}) \tag{18}$$

$$P_{s,k,N}(\mathbf{x}, t) = \sum_{j=1}^{N} P_{s,k,j} \phi_j(\mathbf{x}), \quad k = 2, 3, 4, \quad s = x, y \tag{19}$$

Setting $v_h = \phi_j(\mathbf{x})$ in Equations (13) and (14) on each element K, a system of ODES can be obtained for the expansion coefficient Equations (16) and (19).

DOI: 10.1002/nme

We define the unknown vectors on each element K

$$\mathbf{H}^z = (H_{z,1}, H_{z,2}, \ldots, H_{z,N})^{\mathrm{T}}$$
$$\mathbf{E}^s = (E_{s,1}, E_{s,2}, \ldots, E_{s,N})^{\mathrm{T}}, \quad s = x, y$$
$$\mathbf{Q}^z = (Q_{z,1}, Q_{z,2}, \ldots, Q_{z,N})^{\mathrm{T}}$$
$$\mathbf{P}^{s,k} = (P_{s,k,1}, P_{s,k,2}, \ldots, P_{s,k,N})^{\mathrm{T}}, \quad k = 2, 3, 4, \quad s = x, y$$

and also the basis function vector

$$\boldsymbol{\phi} = (\phi_1, \phi_2, \ldots, \phi_N)^{\mathrm{T}}$$

Using Gauss quadrature formulas to evaluate the integration in Equations (13) and (14) and assuming $\varepsilon_{r,\infty}, \mu_r, \sigma_x, \sigma_y$ constant on each element K, we obtain the following ODEs for the unknown vectors:

$$\frac{\mathrm{d}\mathbf{H}^z}{\mathrm{d}t} = (\mu_r M)^{-1} M^x \mathbf{E}^y - (\mu_r M)^{-1} M^y \mathbf{E}^x - (\mu_r M)^{-1} \int_{\partial K} h_K^{H_z}(\mathbf{U}_N^{(1),-}, \mathbf{U}_N^{(1),+}) \boldsymbol{\phi}(x)\, \mathrm{d}s + \frac{1}{\mu_r} \mathbf{S}_N^{H_z} \tag{20}$$

where

$$\mathbf{S}_N^{H_z} = (S_1^{H_z}, S_2^{H_z}, \ldots, S_N^{H_z})^{\mathrm{T}}$$
$$S_j^{H_z} = -\mu_r d_{0,z} H_{z,j} - \mu_r d_{1,z} Q_{z,j}$$

$$\frac{\mathrm{d}\mathbf{E}^x}{\mathrm{d}t} = -(\varepsilon_{r,\infty} M)^{-1} M^y \mathbf{H}^z - (\varepsilon_{r,\infty} M)^{-1} \int_{\partial K} h_K^{E_x}(\mathbf{U}_N^{(1),-}, \mathbf{U}_N^{(1),+}) \boldsymbol{\phi}(x)\, \mathrm{d}s + \frac{1}{\mu_r} \mathbf{S}_N^{E_x} \tag{21}$$

where

$$\mathbf{S}_N^{E_x} = (S_1^{E_x}, S_2^{E_x}, \ldots, S_N^{E_x})^{\mathrm{T}}$$
$$S_j^{E_x} = -(\varepsilon_{r,\infty} c_{1,x} E_{x,j} + \omega_{\mathrm{p}}^2 P_{x,4,j} + \omega_{\mathrm{p}}^2 c_{1,x} P_{x,3,j} + c_{2,x} P_{x,2,j})$$

$$\frac{\mathrm{d}\mathbf{E}^y}{\mathrm{d}t} = (\varepsilon_{r,\infty} M)^{-1} M^x \mathbf{H}^z - (\varepsilon_{r,\infty} M)^{-1} \int_{\partial K} h_K^{E_y}(\mathbf{U}_N^{(1),-}, \mathbf{U}_N^{(1),+}) \boldsymbol{\phi}(x)\, \mathrm{d}s + \frac{1}{\varepsilon_{r,\infty}} \mathbf{S}_N^{E_y} \tag{22}$$

where

$$\mathbf{S}_N^{E_y} = (S_1^{E_y}, S_2^{E_y}, \ldots, S_N^{E_y})^{\mathrm{T}}$$
$$S_j^{E_y} = -(\varepsilon_{r,\infty} c_{1,y} E_{y,j} + \omega_{\mathrm{p}}^2 P_{y,4,j} + \omega_{\mathrm{p}}^2 c_{1,y} P_{y,3,j} + c_{2,y} P_{y,2,j})$$

$$\frac{\mathrm{d}Q_{z,j}}{\mathrm{d}t} = H_{z,j} \tag{23}$$

DOI: 10.1002/nme

and for $w = x, y$

$$\frac{\mathrm{d}P_{w,2,j}}{\mathrm{d}t} = \omega_{\mathrm{p}}^2 P_{w,3,j} + \varepsilon_{r,\infty} E_{w,j} - \sigma_w P_{w,2,j} \tag{24}$$

$$\frac{\mathrm{d}P_{w,3,j}}{\mathrm{d}t} = P_{w,4,j} \tag{25}$$

$$\frac{\mathrm{d}P_{w,4,j}}{\mathrm{d}t} = E_{w,j} - \gamma P_{w,4,j} \tag{26}$$

Here, M_{ij} is the local mass matrix defined on each element K as

$$M_{ij} = \int_K \phi_i(\mathbf{x})\phi_j(\mathbf{x})\,\mathrm{d}\mathbf{x} \tag{27}$$

and M_{ij}^x and M_{ij}^y are two local stiffness matrices defined as

$$M_{ij}^x = \int_K \frac{\partial \phi_i(\mathbf{x})}{\partial x}\phi_j(\mathbf{x})\,\mathrm{d}\mathbf{x}, \quad M_{ij}^y = \int_K \frac{\partial \phi_i(\mathbf{x})}{\partial y}\phi_j(\mathbf{x})\,\mathrm{d}\mathbf{x} \tag{28}$$

3. CROSS SECTIONS OF AG NANOWIRES ARRAYS AND TIME-DOMAIN BEHAVIOUR

In this section, we will first study the cross sections and time-domain behaviour of coupled plasmon resonant modes for coupled Ag nanowires. The integration path for the calculation of the cross sections [17] is selected to be a circle of large radius r_∞, which will encircle all the Ag cylindrical nanowires. The circle does not have to be very large as all Ag nanowires are placed in the non-absorbing free space.

After choosing the circle with a radius r_∞, we compute the time-averaged Poynting vector $\mathbf{S}$ along this circle by

$$\mathbf{S}_{\mathrm{sca}} = \tfrac{1}{2} Re\{\mathbf{E}_{\mathrm{sca}} \times \mathbf{H}_{\mathrm{sca}}^*\}, \quad \mathbf{S}_{\mathrm{ext}} = \tfrac{1}{2} Re\{\mathbf{E}_{\mathrm{i}} \times \mathbf{H}_{\mathrm{sca}}^* + \mathbf{E}_{\mathrm{sca}} \times \mathbf{H}_{\mathrm{i}}^*\}$$

where subscript $_{\mathrm{sca}}$ represents scattering, $_{\mathrm{i}}$ represents input and $_{\mathrm{ext}}$ represents extinction, all the variables are functions of frequency, obtained by Fourier transform from the time-domain. Then we compute the following values:

$$W_{\mathrm{sca}} = \int_A \mathbf{S}_{\mathrm{sca}} \cdot \hat{\mathbf{e}}_r \,\mathrm{d}A, \quad W_{\mathrm{ext}} = -\int_A \mathbf{S}_{\mathrm{ext}} \cdot \hat{\mathbf{e}}_r \,\mathrm{d}A, \quad W_{\mathrm{abs}} = W_{\mathrm{ext}} - W_{\mathrm{sca}}$$

where $_{\mathrm{abs}}$ represents absorption, and the integration is done along the circle and $\hat{\mathbf{e}}_r$ is the outward unit normal to the circle. Finally, we get the cross sections:

$$C_{\mathrm{ext}} = \frac{W_{\mathrm{ext}}}{I_{\mathrm{i}}}, \quad C_{\mathrm{abs}} = \frac{W_{\mathrm{abs}}}{I_{\mathrm{i}}}, \quad C_{\mathrm{sca}} = \frac{W_{\mathrm{s}}}{I_{\mathrm{i}}}$$

where I_{i} is the incident irradiance.

DOI: 10.1002/nme

For the computation, we use curved triangles to describe the circle exactly, a curved triangle can be mapped by an isoparametric transformation [19] onto a reference triangle $\{(x, y)|, 0\leqslant x, y\leqslant 1, 0\leqslant x + y\leqslant 1\}$. We set the UPML parameters $R(0) = \exp(-16), m = 3$, and fourth-order basis functions (except in the example of exponential convergence analysis) are used for the space discretization and a fourth-order Runge–Kutta method for the time integration. Finally, a pulse input described in Reference [21] is used for computing cross sections.

3.1. An isolated nanowire

First we discuss TE scattering off a single Ag nanowire with radius $r = 25\,\text{nm}$, in which case the analytical solution is known [17]. We will demonstrate an exponential convergence of the DGTD method. All results presented in this paper use Drude parameters from Lynch–Hunter [22]

$$\varepsilon_{r,\infty} = 8.926, \quad \omega_\text{p} = 11.585\,\text{eV}, \quad \gamma = 0.203\,\text{eV}$$

Figure 1 and Table I give a convergence analysis of the DGTD method. An exponential convergence is obtained in Figure 1 and it is more accurate than the FDTD results from Reference [5] while in Table I a pth order convergence error is obtained that L_2 error $= O(\Delta x^p)$. Figure 2 gives a comparison of the analytical cross sections and numerical cross sections on a mesh $\Delta x = 5\,\text{nm}$ with a 5 cell UPML with a thickness of 25 nm.

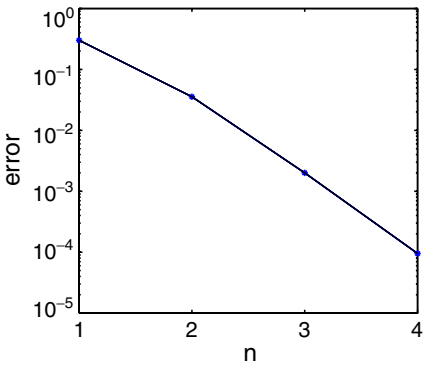

Figure 1. Exponential convergence: error of SCS as a function of the order of basis functions (single Ag nanowire $r = 25\,\text{nm}$, $\Delta x = 2.5\,\text{nm}$).

Table I. Convergence analysis of SCS of one Ag cylinder with radius $r = 25\,\text{nm}$.

Mesh size	L^2 error	Order
$\Delta x = 10\,\text{nm}$ 3-cell UPML	3.57e-2	—
$\Delta x = 5\,\text{nm}$ 5-cell UPML	1.33e-3	4.75
$\Delta x = 2.5\,\text{nm}$ 10-cell UPML	9.531e-5	3.80

DOI: 10.1002/nme

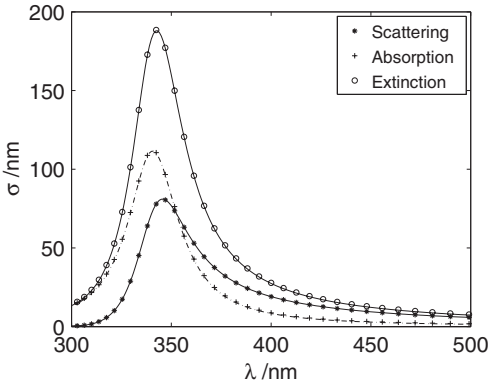

Figure 2. Comparison of analytical (smooth curves) and DGTD numerical (symbols, $\Delta x = 5$ nm) cross sections for a single circular Ag nanowire of radius 25 nm.

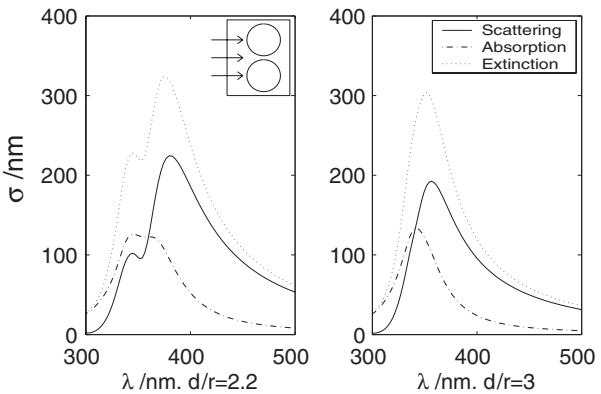

Figure 3. Cross sections for two $r = 25$ nm circular Ag nanowires.

3.2. Linear arrays of Ag nanowires

We consider two kinds of illuminations here, illumination normal to the axis of Ag nanowires and parallel to it. Here r is the radius of nanowires and d is the distance between the centres of Ag nanowires.

- Normal illumination

  Figure 3 presents cross sections for two $r = 25$ nm nanowires with two different spacings d. For the case of $d/r = 2.2$, in addition to the one weak maximum close to the resonance of an isolated nanowire, an additional stronger resonance due to the interaction of the nanowires is present. When $d/r = 3$, the separations is increased, as a result, cross sections are similar to that of isolated nanowire case but with bigger magnitude. Figure 4 presents cross sections for four $r = 25$ nm nanowires with different spacing d. Compared to two nanowire case, cross

DOI: 10.1002/nme

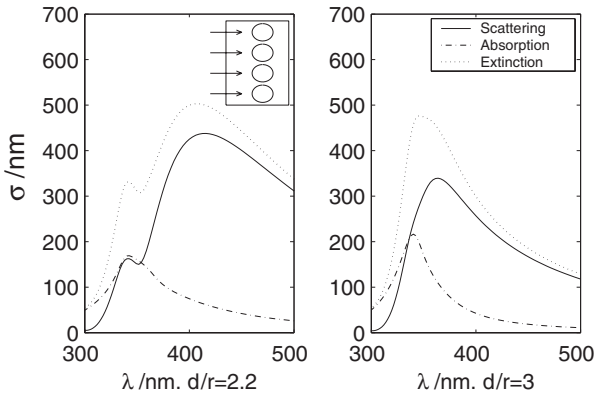

Figure 4. Cross sections for four $r = 25$ nm circular Ag nanowires.

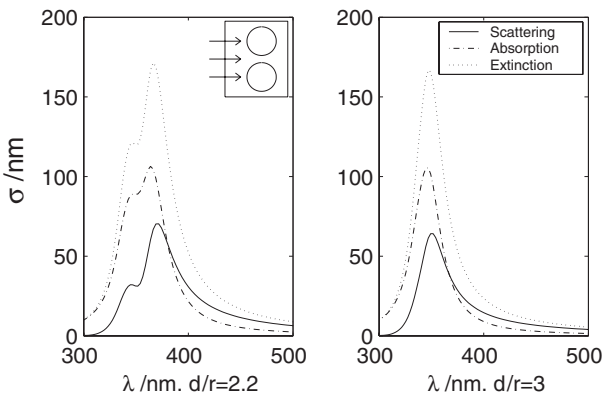

Figure 5. Cross sections for two $r = 15$ nm circular Ag nanowires.

sections for the four nanowire case are larger, and the stronger resonance is wider and red-shifted more.

Figure 5 shows the results for two nanowires with smaller radius, $r = 15$ nm, our results show clearly distinguished secondary resonance, which is missing in the FDTD results from Reference [5]. This is due mainly to the higher-order accuracy of the DGTD method which captures the interaction through the evanescent fields.

- Parallel illumination

  Retardation is essential for the case of parallel incident illumination [23]. We will consider nanowire with $r = 25$ nm and $d/r = 2.2$. Figure 6 gives scattering cross section for different nanowire numbers. Figure 7 give the dependence of the main resonance on the numbers of nanowires, the main resonance red-shifted when nanowire number increases.

DOI: 10.1002/nme

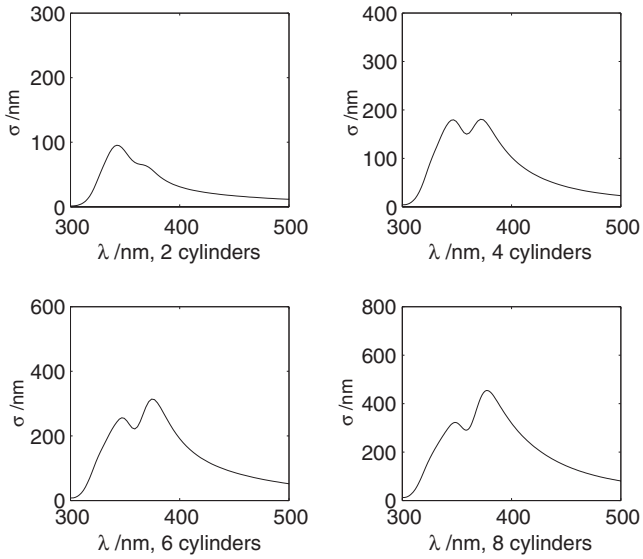

Figure 6. Scattering cross section.

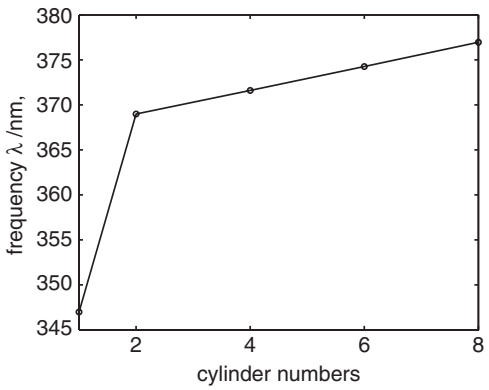

Figure 7. Collective plasmon resonance frequency for $r = 25$ nm circular Ag nanowire arrays of different lengths.

3.3. Time-domain behaviour of complex structures

To demonstrate the capability of the DGTD method, we apply it to study the time-domain behaviour of light in a funnel of nanowires feeding into a double chain array, a configuration of same parameters suggested in Reference [5]. Figure 8 gives time sequence of the magnitude of the electric field with a $\lambda = 448$ nm pulse. Figure 9 plots time-averaged flux across two representative lines, the results agree qualitatively with the results in Reference [5]. Here, we have used $L = 25$ nm for the length non-dimensionalization and the origin of co-ordinate is placed at the centre of the channel mouth.

DOI: 10.1002/nme

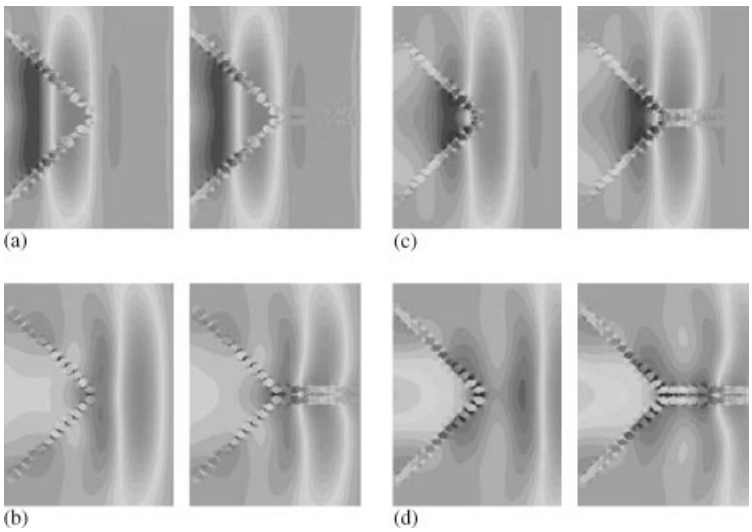

Figure 8. Time sequence of the magnitude of the electric field as a pulse of light interacts with the funnel only (left), and with a funnel and a double chain attached: (a) $T = 25$; (b) $T = 30$; (c) $T = 35$; and (d) $T = 40$ (non-dimensionalized time).

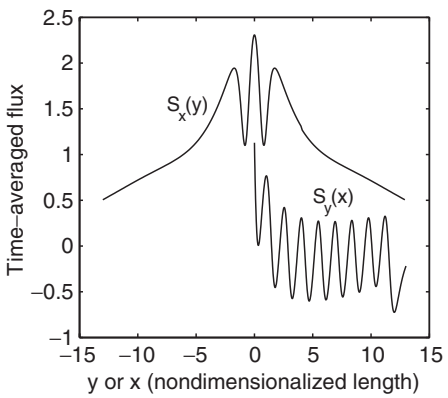

Figure 9. Time-averaged flux, $S_x(y)$ is obtained along a y-direction line 0.8 from the last nanowire centres of the double chain, $S_y(x)$ is along an x-direction line 0.8 from the upper chain nanowire centres.

4. ENERGY LOSS OF RESONANT MODES IN A LINEAR CHAIN

An important issue for the study of coupled nanowires for circuit application is the attenuation of energy transport. Here we investigate the electromagnetic energy transport via linear metal chains in this section. First, we find the resonance frequency ω_c of one nanowire by calculating its scattering cross section, then use a pulse centred at that frequency to illuminate the first nanowire

DOI: 10.1002/nme

only in a linear chain (illumination direction is shown in the inset of pictures). Next, we record the time history of the fields at some selected space locations, using the Fourier transformation in time, we can compute the intensity $I(r, \omega_c) = |E(r, \omega_c)|^2$ at those space locations. As a result, the transmission losses can be extracted by a least-square fit of an exponential form $I = I_0 \exp(-\kappa x)$ [3]. Here, the signal-damping coefficient κ gives an estimate of energy loss of resonant mode along a linear chain. In all the examples computed here a chain of ten nanowires is used, we take the field values at identical position of each nanowire shown by the black circles in the insets, the radius of circular nanowire is 25 nm while the overall size of ellipse nanowire is 50 nm × 25 nm.

Figure 10 gives the decay of field intensity of circular nanowire case, the resonance frequency is 346.9847 THz. The vertical axis is intensity at log-scale normalized to the first nanowire's intensity, the signal-damping coefficient κ is shown in Table II. It can be seen that $d/a = 3$ is the optimum case for the least attenuation per nanometer, where a is the radius of the circular nanowire.

Figure 11 gives the decay of field intensity of ellipse nanowires with the short axis of the ellipse aligning with the direction of the chain, the resonance frequency is 333.7157 THz for the given illumination direction. The vertical axis is intensity at log-scale normalized to the first nanowire's intensity, the signal-damping coefficient κ is shown in Table III, which shows that $d/a = 3$ is again the optimum case, where a is the ellipse radius in the chain direction.

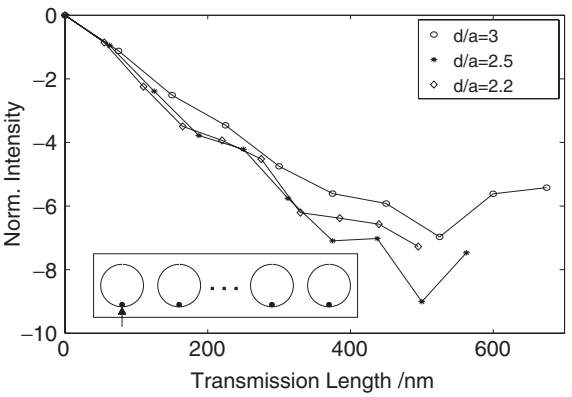

Figure 10. Decay of field intensity in the chain direction, we take the values at identical position of each nanowire shown by the black circle in the inset, the arrow is the illumination direction. The parameter d/a is the ratio of inter-nanowire (centre–centre) distance and nanowire radius.

Table II. Signal-damping coefficient κ for the nanowire chain for different ratios of inter-nanowire distances and nanowire radius.

d/a	$\kappa(\text{nm})^{-1}$	$\kappa(\text{nanowire})^{-1}$
2.2	0.0179	0.9869
2.5	0.0187	1.1687
3	0.0138	1.0348

DOI: 10.1002/nme

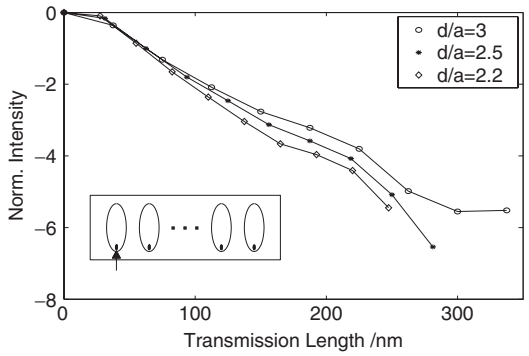

Figure 11. Decay of field intensity in the chain direction, we take the values at identical position of each ellipse shown by the black circle in the inset, the arrow is the illumination direction. The parameter d/a is the ratio of inter-nanowire (centre–centre) distance and ellipse radius in the chain direction.

Table III. Signal-damping coefficient κ for the ellipse chain for different ratios of inter-nanowire distances and ellipse radius (in the chain direction).

d/a	$\kappa(\text{nm})^{-1}$	$\kappa(\text{nanowire})^{-1}$
2.2	0.0239	0.6568
2.5	0.0207	0.6477
3	0.0177	0.6634

Figure 12 gives the decay of field intensity along a chain of ellipse nanowire with the long axis of the ellipse aligning with the direction of the chain, the resonance frequency is 363.8638 THz. Again, the vertical axis is intensity at log-scale normalized to the first nanowire's intensity. The signal-damping coefficient κ is shown in Table IV and $d/a = 3$ is the optimum case, where a is the ellipse radius in the chain direction.

Finally, we consider a chain of ellipse nanowires rotated 45°. Figure 13 gives the decay of field intensity while the resonance frequency is 363.8638 THz. The vertical axis is intensity at log-scale normalized to the first nanowire's intensity. The signal-damping coefficient κ is shown in Table V and $d/a = 3$ is the optimum case, where $a = \sqrt{(r_a^2 + r_b^2)/2}$, r_a, r_b are the long and short axis of the ellipse nanowire, respectively.

Discussion of results. Based on the simulation results above, Figure 14 shows the optimum decays obtained for $d/a = 3$ for four different chains of circular and ellipse nanowires. It can be seen in the case of linear chain of ellipse nanowires, the one where the long axis of the ellipse aligning with the chain direction has the least decay rate, $\kappa = 0.0106\ (\text{nm})^{-1}$ while the one with the short axis of the ellipse aligning with the chain direction has the largest decay rate, $\kappa = 0.0177\ (\text{nm})^{-1}$. The improvement of the rate is about 40. The chain of ellipse nanowire rotated 45° is about the same as the chain of circular nanowires, namely, $\kappa = 0.0140\ (\text{nm})^{-1}$ and $\kappa = 0.0138\ (\text{nm})^{-1}$, respectively, which implies chain of rotated ellipse nanowire can be identified with a chain of effective circular nanowires.

DOI: 10.1002/nme

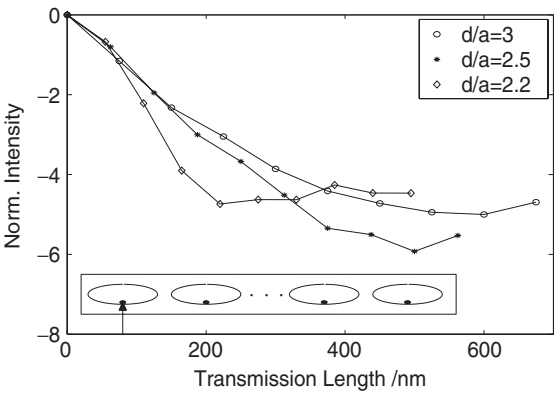

Figure 12. Decay of field intensity in the chain direction, we take the values at identical position of each ellipse shown by the black circle in the inset, the arrow is the illumination direction. The parameter d/a is the ratio of inter-nanowire (centre–centre) distance and ellipse radius in the chain direction.

Table IV. Signal-damping coefficient κ for the ellipse chain for different ratios of inter-nanowire distances and ellipse radius (in the chain direction).

d/a	$\kappa(\text{nm})^{-1}$	$\kappa(\text{nanowire})^{-1}$
2.2	0.0158	0.8688
2.5	0.0144	0.8994
3	0.0106	0.7935

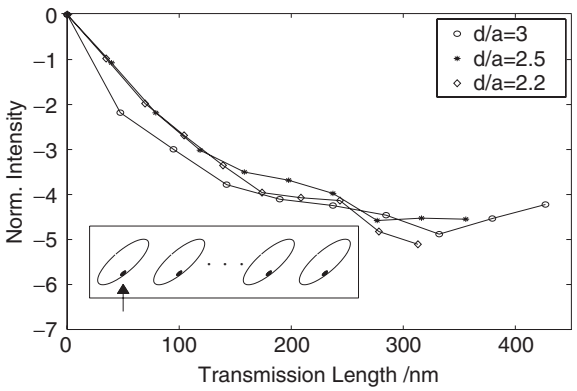

Figure 13. Decay of field intensity in the chain direction, we take the values at identical position of each ellipse shown by the black circle in the inset, the arrow is the illumination direction. The parameter d/a is the ratio of inter-nanowire (centre–centre) distance and $a=\sqrt{(r_a^2+r_b^2)/2}$, here r_a, r_b are the long and short axis of the ellipse nanowire, respectively.

DOI: 10.1002/nme

Table V. Signal-damping coefficient κ for the ellipse chain for different ratios of inter-nanowire distances and $a = \sqrt{(r_a^2 + r_b^2)/2}$, here r_a, r_b are the long and short axis of the ellipse nanowire, respectively.

d/a	$\kappa(\text{nm})^{-1}$	$\kappa(\text{nanowire})^{-1}$
2.2	0.0201	0.6983
2.5	0.0167	0.6596
3	0.0140	0.6649

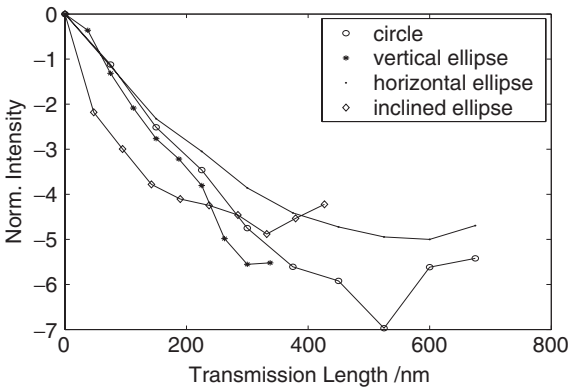

Figure 14. Decay of field intensity in the chain direction with $d/a = 3$.

5. CONCLUSIONS

We have demonstrated high-order accuracy of the DGTD method of dispersive Maxwell's equations for the study of the plasmon resonant coupling of silver nanowires. The capability of the DGTD for handling dispersive materials, arbitrary nanowire geometry, and evanescent fields of the plasmon coupling allows us to obtain clearly resolved information about the resonant frequencies of coupled metal nanowires than the traditional Yee scheme FDTD method. Also, we have shown that the energy decay rate along chain of nanowires depends on the orientation of the ellipse nanowires. We plan to extend these results to 3D cases where the nanowire has finite length.

ACKNOWLEDGEMENTS

Wei Cai would like to thank the support of the National Science Foundation (grant number: DMS-0408309, CCF-0513179) and Department of Energy (Grant Number: DEFG0205ER25678) for the work reported in this paper. P. Zhang acknowledges support from by National Science Foundation of China 90207009 and for Distinguished Young Scholars 10225103.

DOI: 10.1002/nme

REFERENCES

1. Yariv A, Xu Y, Lee RK, Scherer A. Coupled-resonator optical waveguide: a proposal and analysis. *Optical Letters* 1999; **24**:711–713.
2. Takahara J, Kobayashi T. Low-dimensional optical waves and nano-optical circuits. *Optics and Photonics News* 2004; 54–59.
3. Quinten M, Leitner A, Krenn JR, Aussenegg FR. Electromagnetic energy transport via linear chains of silver nanoparticles. *Optical Letters* 1998; **23**:1331–1333.
4. Krenn JR, Dereux A, Weeber JC, Bourillot E, Lacroute Y, Goudonnet JP. Squeezing the optical near-field zone by plasmon coupling of metallic nanoparticles. *Physical Review Letters* 1999; **82**:2590–2593.
5. Gray SK, Kupka T. Propagation of light in metallic nanowire arrays: finite-difference time-domain studies of silver 11 cylinders. *Physical Review B* 2003; **68**:045415-1–045415-11.
6. Kottmann JP, Martin OJF. Plasmon resonant coupling in metallic nanowires. *Optical Express* 2001; **12**:655–663.
7. Kottmann JP, Martin OJF, Smith DR, Schultz S. Dramatic localized electromagnetic enhancement in plasmon resonant nanowires. *Chemical Physics Letters* 2001; **341**:1–6.
8. Kottmann JP, Martin OJF, Smith DR, Schultz S. Plasmon resonances of silver nanowires with a nonregular cross section. *Physical Review B* 2001; **64**:235402-1–235402-10.
9. Stockmann MI, Faleev SV, Bergman DJ. Coherent control of femtosecond energy localization in nanosystems. *Physical Review Letters* 2002; **88**:067402-1–067402-4.
10. Stockmann MI, Faleev SV, Bergman DJ. Coherently controlled femtosecond energy localization on nanoscale. *Applied Physics B*: *Lasers Opticals* 2002; **74**(Suppl.):S63–S67.
11. Lu T, Zhang P, Cai W. Discontinuous Galerkin methods for dispersive and lossy Maxwell's equations. *Journal of Computational Physics* 2004; **200**:549–580.
12. Hesthaven JS, Warburton TC. Nodal high-order methods on unstructured grids—1. Time-domain solution of Maxwell's equations. *Journal of Computational Physics* 2002; **81**:186–221.
13. Xiao T, Liu QH. Three-dimensional unstructured-grid discontinuous Galerkin method for Maxwell's equations with well-posed perfectly matched layer. *Microwave and Optical Technology Letters* 2005; **46**:459–463.
14. Taflove A, Hagness SC. *Computational Electromagnetics*: *The Finite-Difference Time-Domain Method* (2nd edn). Artech House: Boston/London, 2000.
15. Maier SA, kik PG, Atwater HA. Observation of coupled plasmon-polariton modes in Au nanoparticle chain waveguides of different lengths: estimation of waveguide loss. *Applied Physics Letters* 2002; **81**:1714–1716.
16. Brongersma ML, Hartman JW, Atwater HA. Electromagnetic energy transfer and switching in nanoparticle chain arrays below the diffraction limit. *Physical Review B* 2000; **62**:R16356–R16359.
17. Bohren CF, Huffman DR. *Absorption and Scattering of Light by Small Particles* (2nd edn). Wiley: New York, 1983.
18. Sakoda K. *Optical Properties of Photonic Crystals*. Springer: Berlin, Heidelberg, 2001.
19. Szabo B, Babuska I. *Finite Element Analysis*. Wiley: New York, 1991.
20. Mohammadian AH, Shankar V, Hall WF. Computation of electromagnetic scattering and radiation using a time-domain finite-volume discretization procedure. *Computer Physics Communications* 1991; **68**:175–196.
21. Ji X, Lu T, Cai W, Zhang P. Discontinuous Galerkin time domain (DGTD) methods for the study of 2-D waveguide coupled microring resonators. *Journal of Lightwave Technology* 2005; **23**:3864–3874.
22. Lynch DW, Hunter WR. *Handbook of Optical Constants of Solids*. Academic Press: Orlando, 1985.
23. Kottmann JP, Martin OJF. Retardation-induced plasmon resonances in coupled nanoparticles. *Optical Letters* 2001; **26**:1096–1098.

DOI: 10.1002/nme